Xingyi Tang
Department of Mechanics and Engineering Science,
College of Engineering,
Peking University,
Beijing 100871, China
e-mail: x.y.tang@pku.edu.cn

Jianxiang Wang[1]
Department of Mechanics and Engineering Science,
College of Engineering,
CAPT-HEDPS and IFSA Collaborative Innovation Center of MoE,
Peking University,
Beijing 100871, China
e-mail: jxwang@pku.edu.cn

Xin Yi[1]
Department of Mechanics and Engineering Science,
BIC-ESAT, College of Engineering,
Peking University,
Beijing 100871, China
e-mail: xyi@pku.edu.cn

Force Barrier for Lipid Sorting in the Formation of Membrane Nanotubes

Understanding lipid sorting of multicomponent cell membranes associated with tubular deformation is of essential importance to many cell activities such as filopodial growth and protein-mediated vesiculation. Here, we conduct theoretical analysis to investigate how the membrane tubulation induced by an external pulling force over a finite region is regulated by the coupling between the lipid composition and the membrane bending rigidity and tension. It is shown that the presence of the lipid-disordered phase facilitates the nanotube formation by reducing the force barrier. As the pulling region size and the membrane tension increase, the membrane tubulation becomes discontinuous regardless of the coupling effect. The direct proportional relationships between the maximum pulling force and size of pulling region at different coupling scenarios are identified. Analytical solutions for the linear force-extraction relation and the membrane configurations in the early stage of the membrane extraction are obtained. Our results indicate that in the case of a relatively small pulling region, the coupling between the membrane composition and mechanical properties plays an important role in regulating the membrane extraction, and such an effect due to the phase separation diminishes gradually as the pulling region enlarges and the force barrier becomes dominated by a large pulling region.
[DOI: 10.1115/1.4044385]

Keywords: lipid sorting, membrane tubulation, multicomponent membrane, lipid composition coupling, pulling region size, force barrier, phase separation

1 Introduction

Biological membranes consist of different types of lipid molecules, sphingomyelin, and cholesterol. Owing to the free motion of these molecules in the membrane plane, the multicomponent membranes could laterally organize into rafts and micro-domains and exhibit complex morphology. For example, ternary lipid mixtures could undergo phase separation into two coexisting fluid phases with clear domain structures, one with a large and the other with a low cholesterol molar fraction [1,2]. It is demonstrated that the phase separation and selective incorporation of specific proteins within domains regulate the protein functions [3], membrane deformation [2], budding transition [4], and vesicle fission, which play essential roles in many cellular activities including the membrane signaling, trafficking, sorting processes, endocytosis, and exocytosis [5]. In budding yeast, protein clusters containing activated Cdc42 could be formed and activated Cdc42 concentrates at a site on the cell membrane where the bud eventually emerges [6]. Clathrin-mediated endocytosis exhibits complex behaviors of phase separation and membrane reshaping [7]. Moreover, depending on the local composition of the membrane, phase-separated domains prefer regions of certain local membrane curvatures, suggesting lipid sorting aided by membrane curvatures [8]. For a vesicle with multiple lipid phases, it could adopt stable morphologies with several disconnected flexible liquid-disordered (L_d) domains embedded in a more stiff multiply-connected liquid-ordered (L_o) domain, in which the flexible L_d domains have large curvature and the relatively stiff L_o domains bend weakly, lowering the bending energy of the vesicle [1,2,4]. Further numerical studies indicate that volume constraints of the vesicle and the difference in the Gaussian curvature moduli of the lipid phases could facilitate the formation of the multidomain morphologies [4]. Curvature-based sorting of lipid phases has also been observed in supported lipid bilayers on patterned or templated substrates with varying curvatures, where fluorescent lipids have been used as trafficking markers [9,10]. For example, stiffer L_o domains prefer to partition into the flat regions and more flexible L_d domains into the curved regions [9,10]. Similarly, sorting of peripheral proteins takes place on substrate-supported wavy lipid membranes [11].

In addition to round vesicles and membrane patches, sorting of lipid phases has also been observed in lipid membrane nanotubes which are ubiquitous in living cells and their organelles and play an important role in numerous cell activities including intra- and intercellular transport [12], communication, endocytosis [7], and cell migration [13]. As a tubular structure or protrusion, lipid membrane nanotubes have a simple geometry with a typical diameter of tens of nanometers but could exhibit strong coupling between the curvature and membrane composition. It is reported that periodic membrane tubes could adopt a necklace-like shape and undergo a complete phase separation with the L_d phase in the neck region while the L_o phase in the bulge region of each oblate subunit [2]. Previous experimental studies show that L_d domains nucleated in membrane nanotubes pulled from giant vesicles in ternary mixtures in quasi-static pulling circumstances [14,15]. Similar results have been obtained in theoretical analysis on the membrane nanotube formation at a local point pulling force, considering the coupling between the membrane composition and the membrane bending rigidity and tension [16]. Further experimental and theoretical investigations show that the lipid sorting in membrane tubes also highly depend on the pulling speed [17,18]. Besides studies on the extraction of purified lipid membranes, it is demonstrated recently that the BAR protein scaffold bounding to an underlying elongated membrane nanotube could generate a lipid mobility barrier which increases the membrane tension and eventually induces the tube rupture through lysis [19].

In real situations, the external pulling force required for the nanotube formation in vivo is applied on a pulling region of a finite size,

[1]Corresponding authors.

Contributed by the Applied Mechanics Division of ASME for publication in the Journal of Applied Mechanics. Manuscript received May 21, 2019; final manuscript received July 26, 2019; published online August 1, 2019. Assoc. Editor: Yashashree Kulkarni.

which includes attachment domains for a cluster of molecular bonds or motors [20,21], protein scaffolding [22], and the tip region of polymerizing cytoskeletal filaments [23,24]. However, in most existing theoretical work, a scenario of a point pulling force is widely assumed to approximate the actual finite pulling region [16,18,25,26]. Only for a homogeneous membrane, few studies based on experiments, computational simulations, and continuum modeling in quasi-static pulling circumstance have been performed to investigate the size effect of the pulling region on the membrane extraction [20,27–30].

Though significant progress has been made in understanding the formation and pulling behaviors of the multicomponent membrane tubes, the effects of the pulling region size on the membrane extraction and possible lipid sorting remain unclear. In this work, we perform theoretical analysis under a continuum modeling framework to explore the interplay of lipid composition and curvature in membrane tubes as well as the size dependence of the relationship between the pulling force and membrane extraction. It is shown that the presence of the L_d phase facilitates the nanotube formation by reducing the force barrier. As the pulling region size and the membrane tension increase, the force-extraction curve becomes discontinuous, and a discontinuous membrane shape transformation from a catenoid-like shape to a tubular structure is observed. Such a discontinuous shape transformation might occur at certain coupling scenarios once the maximum pulling force is achieved. We also investigate how the phase separation depends on the membrane tension. The direct proportional relationships between the maximum pulling force and size of the pulling region at different coupling scenarios are identified. Moreover, analytical solutions for the force-extraction relation and the membrane configuration in the early extraction stage are obtained based on a general force balance of the nonlinearly deformed membrane.

2 Modeling and Methods

In the adopted cylindrical coordinate (r, θ, z), we consider an initially flat circular membrane of lipid mixtures undergoing an axisymmetric deformation induced by an external pulling force f acting on a circular region along the z-axis as shown in Fig. 1. The radial sizes of the membrane patch and pulling region are R and r_p, respectively. This model lipid membrane is composed of unsaturated and saturated lipid molecules (along with other types of molecules) forming two coexisting fluid phases, the liquid-disordered (L_d) phase rich in unsaturated (red) lipids and the liquid-ordered (L_o) phase rich in saturated (blue) lipids (see Fig. 1). A typical example is a lipid membrane consisting of a ternary mixture of unsaturated dioleoylphosphatidylcholine (DOPC), saturated sphingomyelin (SM), and cholesterol (Chol) which can separate into distinct domains at 290 K. To characterize the free energy of the domain structure, an order parameter $\phi = (c_1 - c)/(c_1 - c_2)$ is introduced with c_1 and c_2 as the concentrations of the unsaturated lipids in the L_d phase and L_o phase, respectively, and $c \in [c_2, c_1]$ as the local concentration of the unsaturated lipids. At $\phi = 0$ (or $c = c_1$), the local membrane domain is in the L_d phase, while the local membrane domain is in the L_o phase at $\phi = 1$. In general, unsaturated lipid molecules are of relatively larger lateral area per molecule and shorter chains in comparison with saturated lipid molecules, leading to a more flexible lipid domain in the L_d phase [14].

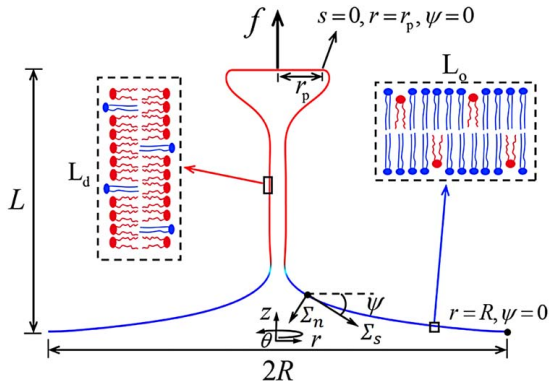

Fig. 1 Schematic of the extraction of a mixture membrane induced by an exterior force f on a circular pulling region of radius r_p in the adopted cylindrical coordinate (r, θ, z). s and ψ denote the arclength and tangent angle of the membrane profile with phase L_d colored red (the tubular region) and phase L_o colored blue (the lower region). The tangent angle ψ is positive as measured clockwise from the positive r-axis. Σ_n and Σ_s, defined in Eq. (1), denote the out-of-plane shear force and in-plane force, respectively. Insets illustrate the enlarged structures of the local membrane domains. (Color version online.)

The elastic deformation energy of the axisymmetric membrane is given by the Canham-Helfrich membrane theory as [31]

$$E_1 = 2\pi \int \left[\frac{\kappa(\phi)}{2} (C_1 + C_2)^2 + \sigma(\phi) \right] r \mathrm{d}s$$

where $C_1 = \mathrm{d}\psi/\mathrm{d}s$ and $C_2 = \sin\psi/r$ represent the principal curvatures in the meridional and circumferential directions, respectively, with s and ψ denoting the arclength and tangent angle of the membrane profile (Fig. 1). The bending rigidity $\kappa(\phi)$ and tension $\sigma(\phi)$ of the membrane are functions of the local composition ϕ. Here, we adopt $\kappa(\phi) = \kappa_0[1 - \alpha(1 - \phi^2)]$ with $\alpha > 0$ and $\sigma(\phi) = \sigma_0[1 - \beta(1 - \phi^2)]$ as introduced in Ref. [16]. In the L_o phase, $\kappa = \kappa_0$ and $\sigma = \sigma_0$, whereas $\kappa = \kappa_0(1 - \alpha)$ and $\sigma = \sigma_0(1 - \beta)$ in the L_d phase. Experiments on the lipid segregation in the SM:Chol:DOPC vesicles suggest that a reasonable value for the coupling parameter α could be around 0.5 [2,14]. For example, at a molar ratio of 1:1:0 of SM:Chol:DOPC, an L_o phase is observed, and the membrane bending rigidity is $\kappa(\phi = 1) = \kappa_0 = 65 \pm 6\ k_B T$ with the thermal energy $1\ k_B T = 4.11 \times 10^{-21}$ J, while an L_d phase is observed with $\kappa(\phi = 0) = \kappa_0(1 - \alpha) = 30 \pm 3\ k_B T$ for the 0:1:1 membrane composition [2,14]. Hereinafter, we take $\alpha = 0.5$ in the case of the membrane composition coupling to bending rigidity. The coupling parameter β could be positive or negative. For instance, it is reported that the lateral tension of the SM:Chol:DOPC membrane in the L_d and L_o phases is $\sigma(\phi = 0) = 8.2 \pm 0.1 \times 10^{-5}$ mN/m and $\sigma(\phi = 1) = 1.06 \pm 0.01 \times 10^{-4}$ mN/m, respectively [2], which suggests $\beta = 0.23$; while other experiments indicate that the tension of the lipid domain in the L_d phase could be five times less than that in the L_o phase [17]. The effects of the spontaneous curvature and Gaussian rigidity on the lipid domain configuration are not considered [32,33]. We have also omitted the pressure difference across the membrane as it plays a negligible role in the membrane nanotube formation [25,26].

The phase separation is analyzed within the Ginzburg–Landau free energy functional as [16,32,34]

$$E_2 = 2\pi \int \left[\frac{\lambda}{2} \phi^2 (1 - \phi)^2 + \frac{\mu}{2} \left(\frac{\partial \phi}{\partial s} \right)^2 \right] r \mathrm{d}s$$

where λ and μ are positive material constants arising from the intermolecular interactions and their combination gives a characteristic length $\sqrt{\mu/\lambda}$ determining the thickness of the interface transition domain and a line tension of a characteristic value $\sqrt{\lambda\mu}$ in the transition domain; s is the arclength of the membrane profile initiating from the boundary of the pulling region. Here, we assume that the membrane connects to a lipid reservoir and the number of lipid molecules is not conserved. In our calculations, $\lambda = 2000\ \kappa_0/R^2$ and $\mu = \kappa_0$.

With the geometric relations $\mathrm{d}r/\mathrm{d}s = \cos\psi$ and $\mathrm{d}z/\mathrm{d}s = -\sin\psi$, E_1 and E_2 can be expressed as functions of ϕ and ψ. The total free energy of the system is now given as $E_{tot}(\phi, \psi) = E_1 + E_2 - fL$ with L as the displacement of the pulling force f along the z-direction.

To obtain the minimum state of $E_{tot}(\phi(s), \psi(s))$ at a given force displacement L, we employ the interior point optimization technique to numerically determine the corresponding unknown variables ϕ and ψ. As shown in Fig. 1, the membrane profile can be

divided into two regions, the flat pulling region and the outer free membrane region. In the pulling region ($r \in [0, r_p]$, $z = L$), $\psi(r) = 0$ and the order parameter $\phi = \phi(r)$ is approximated by a cubic B-spline curve as $\phi(r) = \sum a_i N_i(r)$ ($i = 0, \ldots, m$), where the control points a_i denote coefficients of the basis functions $N_i(r)$ defined on a non-uniform knot of r. For the outer free membrane with an unknown total arclength l_m, we introduce a new variable $t = s/l_m$ ($t \in [0, 1]$), and both $\phi = \phi(s)$ and $\psi = \psi(s)$ ($s \in [0, l_m]$) are reparametrized and approximated as $\phi(t) = \sum b_j N_j(t)$ and $\psi(t) = \sum c_j N_j(t)$ ($j = 0, \ldots, n$) with control points b_j and c_j as coefficients to be determined. Here, we take $m = 54$ and $n = 114$ in our calculations. A relatively large value of m is taken here to ensure the numerical accuracy for the local composition ϕ in the flat pulling region with a zero membrane curvature. Further calculations indicate that the results are not sensitive to the values of m and n, and a much smaller m would not affect the final results.

The boundary conditions are as follows. At $r = 0$ and $z = L$, $d\phi/dr|_{r=0} = 0$ which means that the order parameter ϕ can vary freely at the center of the pulling region [16]. At $s = 0$ ($t = 0$), we have $\psi = 0$, $r = r_p$, $z = L$, and the continuity of ϕ. At the remote boundary $s = l_m$ ($t = 1$), we have $\psi = 0$, $r = R$, $z = 0$, and $\phi_2 = \phi_0$. Here, $\psi(s = l_m) = 0$ approximates the asymptotic flatness of the membrane at the remote boundary. A zero mean curvature at $s = l_m$ is enforced alternatively in some theoretical work [16,25,26]. $\phi(s = l_m) = \phi_0$ implies that the membrane connects to a lipid reservoir in either L_d phase ($\phi_0 = 0$) or L_o phase ($\phi_0 = 1$). As a membrane at $\phi = 0$ has lower system energy and automatically satisfies the boundary condition $\phi_0 = 0$, the lipid separation could not occur at $\phi_0 = 0$ and the membrane stays homogeneous. Therefore, we focus on the case of $\phi_0 = 1$ in the following analysis. We further take $\alpha = 0$ ($\beta = 0$) for no coupling between the membrane composition and bending (tension) and adopt $\alpha = 0.5$ ($\beta = 0.5$) to account for the composition coupling to the membrane bending (tension). With the knowledge of these boundary conditions, the total free energy of the membrane is minimized with respect to the coefficients a_i, b_i, c_i, and l_m, and the corresponding membrane configuration and the pulling force are determined.

3 Results and Discussion

We first investigate the effects of the coupling parameter α and pulling region radius r_p on the membrane extraction at $\beta = 0$. In a special case of a cylindrical membrane nanotube of uniform composition ($\phi = 0$ or 1), the elastic membrane energy is $E_{tube} = 2\pi r L[\kappa/(2r^2) + \sigma]$, where r and L denote the tube radius and length, respectively. Minimizing E_{tube} with respect to r by taking $dE_{tot}/dr = 0$, we could obtain the equilibrium tube radius [25,26]

$$r_0 = \sqrt{\kappa/(2\sigma)}$$

Substituting r_0 into E_{tube}, we then have an equilibrium pulling force f_0 and the corresponding minimum energy E_{tube} as

$$f_0 = (dE_{tube}/dL)|_{r=r_0} = 2\pi\sqrt{2\sigma\kappa} \quad \text{and} \quad E_{tube} = 2\pi L\sqrt{2\sigma\kappa}$$

For the nanotube in L_o phase ($\phi = 1$), we then have $r_0 = \sqrt{\kappa_0/(2\sigma_0)}$ and $f_0 = 2\pi\sqrt{2\sigma_0\kappa_0}$; for the tube in L_d phase ($\phi = 0$), we have $r_{\alpha\beta} = \sqrt{\kappa_0(1-\alpha)/[2\sigma_0(1-\beta)]}$ and $f_{\alpha\beta} = 2\pi\sqrt{2\sigma_0\kappa_0(1-\alpha)(1-\beta)}$. As $\alpha, \beta < 1$, the elastic deformation energy of the nanotube in the L_d phase is smaller than that in the L_o phase.

As shown in Fig. 2(*a*), in the early stage of the membrane extraction, the pulling force f increases almost linearly with the pulling displacement L and then gradually increases to a peak value f_{max}. Once the force barrier is overwhelmed, the catenoid-like outer free membrane region exhibits a slight constriction and begins to form a cylindrical tubular structure (Figs. 2(*b*)–2(*e*)), and the force drops to a plateau force

$$f_{\alpha\beta} = 2\pi\sqrt{2\sigma_0\kappa_0(1-\alpha)(1-\beta)}$$

which is required to maintain the tubule. In comparison with the case of no coupling ($\alpha = \beta = 0$) with the plateau force $f_0 = 2\pi\sqrt{2\sigma_0\kappa_0}$, the phase separation leads to a lower plateau force at $\alpha, \beta < 1$. As L further increases, the tubular structure elongates without conformational variation of other membrane regions, and the pulling force maintains constant. The phenomena discussed above are shared by the cases of either zero or finite α and r_p. Similar f–L profiles are observed in the packing of a nanotube or microtubule in a vesicle which is deformed and exhibits a cherry-like shape with a single tubular protrusion [29,35]. In the case of the coupling of composition and bending rigidity, the phase separation occurs as the extraction displacement L increases. As shown in Figs. 2(*c*) and 2(*e*), the more flexible L_d phase aggregates into the tubular domain of a relatively large local curvature and the catenoidal outer membrane region remains in the L_o phase. Compared with the cases without composition coupling to the bending rigidity ($\alpha = 0$), the membrane at a finite α exhibits smaller peak and plateau forces as the L_d phase is more flexible than the L_o phase (Fig. 2(*a*)). The coupling between the membrane bending rigidity and membrane composition benefits the formation of the membrane nanotube. This is also reflected in the force jump. At $\alpha = 0.5$, the force jump occurs at a smaller L/R and the force overshoot $(f_{max} - f_0)/f_0$ or the magnitude of the force jump increases in

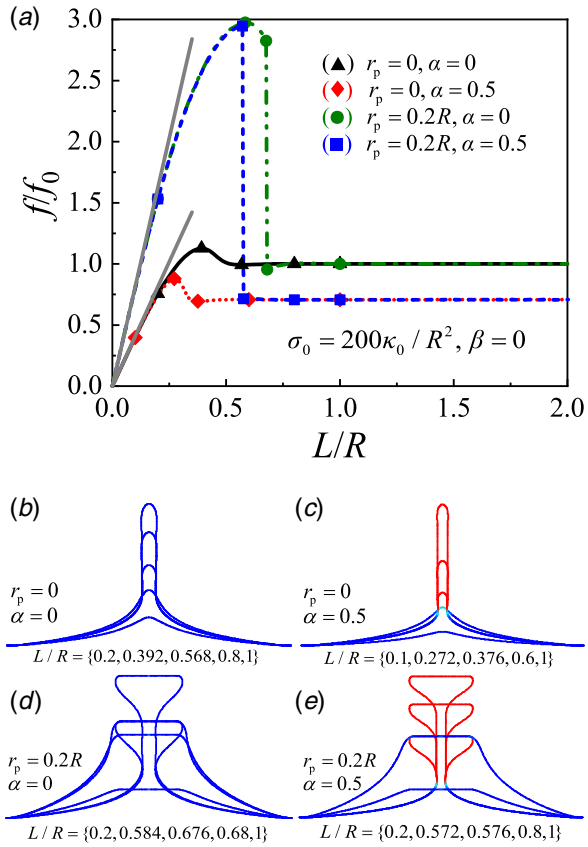

Fig. 2 Effects of the coupling parameter α and the pulling region radius r_p on the membrane extraction at $\sigma_0 = 200\kappa_0/R^2$ and $\beta = 0$. (*a*) Normalized *f*–*L* curves and (*b* – *e*) selected membrane configurations at different α and r_p. The forces correspond to the configurations in (*b* – *e*) are denoted by the symbols in (*a*). The grey solid lines in (*a*) indicate the analytical solutions of the linear *f*–*L* relations at zero and finite r_p. The membranes in (*b*) and (*d*) have no coupling and are in the L_o phase colored blue (or dark grey). In (*c*) and (*e*), the blue (or dark grey) lines represent the membrane domains in the L_o phase and red (or grey) lines the L_d phase. (Color version online.)

comparison with the case of zero α. As the elastic deformation energy of a membrane nanotube of a given length in L_d phase is smaller than that in L_o phase, the membrane nanotube is always in the L_d phase as long as the phase separation occurs. We also calculate the area variation $\varepsilon_A = (A - A_0)/A_0$ during the pulling process with $A_0 = \pi R^2$ and A as areas of the initially flat and deformed membrane. In the case of $r_p = \alpha = 0$ (Fig. 2(*b*)), we have $\varepsilon_A = 0.075$ at $L/R = 0.8$ and $\varepsilon_A = 0.095$ at $L/R = 1$; in the case of $r_p = 0.2R$ and $\alpha = 0.5$ (Fig. 2(*e*)), we have $\varepsilon_A = 0.17$ at $L/R = 0.8$ and $\varepsilon_A = 0.184$ at $L/R = 1$. Including the area contribution from the tubular protrusion and the deformation of the catenoid-like outer membrane region, the small value of ε_A indicates that the area of the nanotube is significantly smaller than that of the whole membrane.

In the above analysis, we perform the full nonlinear analysis based on the angle-arclength parametrization. As shown in Figs. 2(*b*)–2(*e*), in the early extraction stage, f increases almost linearly with the displacement L, and the membrane can be regarded as a homogeneous membrane as no phase separation occurs. These features imply that there might exist a simple analytical solution for the initial linear f–L relation. To seek that analytical prediction, we start the derivation from the balance of the membrane force. For the deformed outer free membrane before phase separation, the local membrane force per unit length can be expressed as [36,37]

$$\Sigma_n = -\kappa_0 \frac{\mathrm{d}(C_1 + C_2)}{\mathrm{d}s} = -\kappa_0 \left(\frac{\mathrm{d}^2\psi}{\mathrm{d}s^2} + \frac{\cos\psi}{r}\frac{\mathrm{d}\psi}{\mathrm{d}s} - \frac{\sin\psi\cos\psi}{r^2} \right)$$

$$\Sigma_s = \sigma_0 + \frac{\kappa_0}{2}(C_2^2 - C_1^2) = \sigma_0 + \frac{\kappa_0}{2}\left[\frac{\sin^2\psi}{r^2} - \left(\frac{\mathrm{d}\psi}{\mathrm{d}s}\right)^2 \right] \tag{1}$$

$$\Sigma_\theta = 2\sigma_0 - \Sigma_s$$

where Σ_n denotes the out-of-plane shear force along the inward normal direction of the deformed membrane, and Σ_s and Σ_θ represent the in-plane force along the meridional and circumferential directions, respectively. In the notation of plate theory, $(\Sigma_n, \Sigma_s, \Sigma_\theta)$ is usually denoted as (Q_n, N_r, N_t) with Q_n named as the shear force, N_r the radial force and N_t the tangential force [38].

The force balance along the z-axis requires that

$$2\pi r\left(\Sigma_s \sin\psi + \Sigma_n \cos\psi\right) = f \tag{2}$$

At small membrane deformation ($L/R \ll 1$ or $\mathrm{d}z/\mathrm{d}r \ll 1$), we have

$$\sin\psi \approx -\frac{\mathrm{d}z}{\mathrm{d}r}, \quad \cos\psi \approx 1, \quad \frac{\mathrm{d}\psi}{\mathrm{d}s} \approx -\frac{\mathrm{d}^2 z}{\mathrm{d}r^2}, \quad \frac{\mathrm{d}^2\psi}{\mathrm{d}s^2} \approx -\frac{\mathrm{d}^3 z}{\mathrm{d}r^3} \tag{3}$$

and then Eq. (1) reduces to

$$\Sigma_n \approx \kappa_0 \left(\frac{\mathrm{d}^3 z}{\mathrm{d}r^3} + \frac{1}{r}\frac{\mathrm{d}^2 z}{\mathrm{d}r^2} - \frac{1}{r^2}\frac{\mathrm{d}z}{\mathrm{d}r} \right)$$

$$\Sigma_s \approx \Sigma_\theta \approx \sigma_0 \tag{4}$$

Substituting Eqs. (3) and (4) into Eq. (2), we have

$$\frac{\mathrm{d}}{\mathrm{d}r}\left[\frac{1}{r}\frac{\mathrm{d}}{\mathrm{d}r}\left(r\frac{\mathrm{d}z}{\mathrm{d}r} \right) \right] = \frac{1}{\kappa_0}\left(\frac{f}{2\pi r} + \sigma_0 \frac{\mathrm{d}z}{\mathrm{d}r} \right) \tag{5}$$

which can be rewritten as a linear modified Bessel differential equation

$$r^2\frac{\mathrm{d}^2}{\mathrm{d}r^2}\left(\frac{\mathrm{d}z}{\mathrm{d}r}\right) + r\frac{\mathrm{d}}{\mathrm{d}r}\left(\frac{\mathrm{d}z}{\mathrm{d}r}\right) - \left(1 + \frac{\sigma_0}{\kappa_0}r^2\right)\frac{\mathrm{d}z}{\mathrm{d}r} = \frac{f}{2\pi\kappa_0}r$$

Equation (5) can also be derived based on the von Karman plate theory widely used in solid mechanics for punching a flat thin film, taking advantage of the assumption of equal radial and tangential forces ($N_r = N_t$) [38–40].

With the boundary conditions $\mathrm{d}z/\mathrm{d}r = 0$ at $r = r_p$ and $r = R$, an analytical solution of $\mathrm{d}z/\mathrm{d}r$ can be found as

$$\frac{\mathrm{d}z}{\mathrm{d}r} = \frac{fR}{2\pi\kappa_0}\frac{1}{\omega^2}\left[\Lambda_1 I_1(\omega\bar{r}) - \Lambda_2 K_1(\omega\bar{r}) - \bar{r}^{-1}\right]$$

where $\bar{r} \equiv r/R$, $\bar{r}_p \equiv r_p/R$, $\omega = \sqrt{\sigma_0 R^2/\kappa_0}$, $\Lambda_0 = I_1(\omega)K_1(\omega\bar{r}_p) - I_1(\omega\bar{r}_p)K_1(\omega)$, $\Lambda_1 = [K_1(\omega\bar{r}_p) - K_1(\omega)/\bar{r}_p]/\Lambda_0$, and $\Lambda_2 = [I_1(\omega\bar{r}_p) - I_1(\omega)/\bar{r}_p]/\Lambda_0$. Here, $I_i(x)$ and $K_i(x)$ ($i = 0, 1, 2$) are the ith order of the first and second kind modified Bessel functions of x, respectively.

As the pulling displacement is L, we have

$$-\int_{r_p}^{R}\frac{\mathrm{d}z}{\mathrm{d}r}\mathrm{d}r = L$$

with the boundary condition $z = 0$ at $r = R$, which then leads to the following linear force-extraction relation

$$f = \frac{2\pi\kappa_0}{R}\frac{\omega^3}{\Lambda_1\left[I_0(\omega\bar{r}_p) - I_0(\omega)\right] + \Lambda_2\left[K_0(\omega\bar{r}_p) - K_0(\omega)\right] - \omega\ln\bar{r}_p}\frac{L}{R} \tag{6}$$

and, in turn, the membrane shape

$$z = -\int_r^R \frac{\mathrm{d}z}{\mathrm{d}r}\mathrm{d}r$$

$$= \frac{fR^2}{2\pi\kappa_0}\frac{1}{\omega^3}\{\Lambda_1[I_0(\omega\bar{r}) - I_0(\omega)] + \Lambda_2[K_0(\omega\bar{r}) - K_0(\omega)] - \omega\ln\bar{r}\} \tag{7}$$

Combining Eqs. (6) and (7), we know that the membrane profile characterized by $z(r)$ is also linearly proportional to L. From the first derivative,

$$\frac{\mathrm{d}f}{\mathrm{d}\bar{r}_p} = \frac{2\pi\kappa_0 L}{R^2}\bar{r}_p\omega^4 g^2(\omega, \bar{r}_p)$$

with $g(\omega, \bar{r}_p)$ as a function of ω and $\bar{r}_p$, we know that the slope of the linear f–L relation increases as $\bar{r}_p$ increases, consistent with the plots in Fig. 3(*a*) showing the linear f–L relation in Eq. (6) as a function of ω at different $\bar{r}_p$. The membrane profiles determined by Eq. (7) for $\bar{r}_p = 0$ and 0.2 at $L/R = 0.1$ and $\omega = 10$ are plotted in Fig. 3(*b*).

It is interesting to note that another linear relation between z and L at small membrane extraction has been reported in a previous theoretical study [25]. In that work, based on an assumption that the membrane portion in the vicinity of the remote boundary ($r \to R$) adopts a catenoid configuration with a prescribed boundary condition of zero moment (or zero mean curvature) at $r = R$, the outer free membrane region is divided into two parts, a catenoid outer part and an inner part which can be determined from a geometric matching condition [25]. No analytical solution on the f–L relation is reported therein [25]. In our current work, both the linear f–L and z–L relations at small membrane deformation (from Eqs. (6) and (7)) are derived analytically, and no additional assumption is required. As shown in Fig. 3(*b*), our theoretical solution agrees well with fully nonlinear numerical solutions.

In the case of a point pulling force ($\bar{r}_p = 0$), Eqs. (6) and (7) reduce to

$$f = \frac{2\pi\kappa_0}{R}\frac{\omega^3 I_1(\omega)}{2 - I_0(\omega) - \omega K_1(\omega) + \omega I_1(\omega)\left(\ln\frac{\omega}{2} + \gamma_E\right)}\frac{L}{R}$$

$$z = \frac{fR^2}{2\pi\kappa_0}\frac{1}{\omega^3}\left\{[1 - \omega K_1(\omega)][I_0(\omega\bar{r}) - I_0(\omega)]{I_1}^{-1}(\omega) - \omega[K_0(\omega\bar{r}) - K_0(\omega) + \ln\bar{r}]\right\}$$

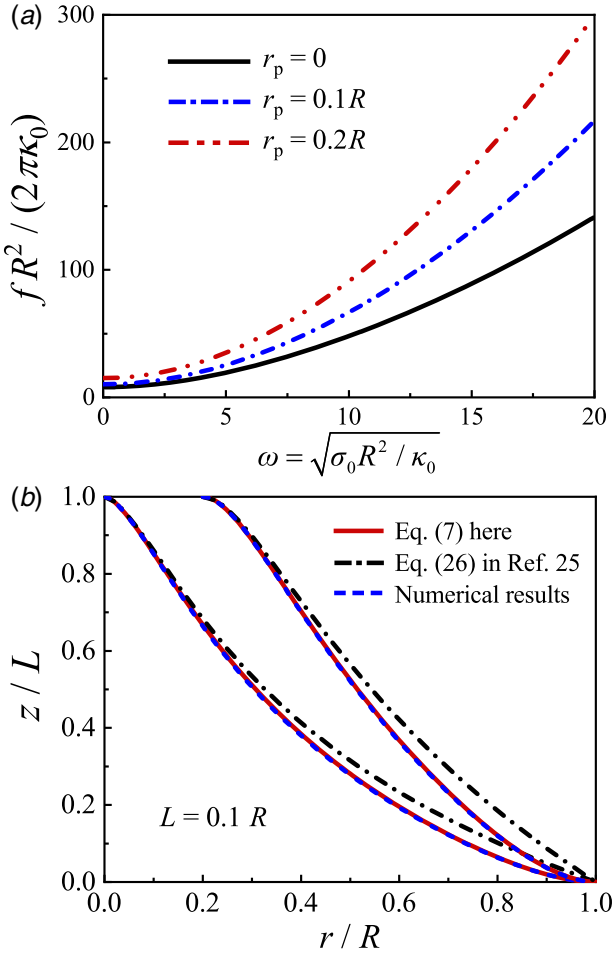

Fig. 3 (*a*) The linear *f*–*L* relation at small membrane deformation given in Eq. (6) as a function of $\omega=\sqrt{\sigma_0 R^2/\kappa_0}$ at different values of r_p. (*b*) Comparison of the rescaled membrane profiles from the current and previous analysis for $r_p = 0$ and $0.2R$ at $L = 0.1R$ and $\omega = 10$. Equation (7) agrees well with the fully nonlinear numerical solutions. (Color version online.)

where $\gamma_E = 0.5772\ldots$ is the Euler–Mascheroni constant. The grey solid lines in Fig. 2(*a*) indicate the analytical solutions of the linear *f*–*L* relations above at zero and finite r_p. The results are consistent with our numerical calculations in the early stage of the membrane extraction.

In the limiting case of zero membrane tension ($\omega = 0$), Eqs. (6) and (7) become

$$f = \frac{16\pi\kappa_0}{R}\frac{1-\bar{r}_p^2}{(1-\bar{r}_p^2)^2 - 4\bar{r}_p^2(\ln\bar{r}_p)^2}\frac{L}{R}$$

$$z = \left[(1-\bar{r}^2+2\bar{r}^2\ln\bar{r}) - \frac{2\bar{r}_p^2\ln\bar{r}_p}{1-\bar{r}_p^2}(1-\bar{r}^2+2\ln\bar{r})\right] \times \frac{(1-\bar{r}_p^2)}{(1-\bar{r}_p^2)^2 - 4\bar{r}_p^2(\ln\bar{r}_p)^2}L \quad (8)$$

leading to

$$z = \left[(1-\bar{r}^2+2\bar{r}^2\ln\bar{r}) - \frac{2\bar{r}_p^2\ln\bar{r}_p}{1-\bar{r}_p^2}(1-\bar{r}^2+2\ln\bar{r})\right]\frac{f R^2}{16\pi\kappa_0} \quad (9)$$

At $\bar{r}_p = 0$, Eq. (8) reduces to

$$f = \frac{16\pi\kappa_0 L}{R^2} \quad \text{and} \quad z = (1-\bar{r}^2+2\bar{r}^2\ln\bar{r})L$$

giving rise to

$$z = \frac{f R^2}{16\pi\kappa_0}(1-\bar{r}^2+2\bar{r}^2\ln\bar{r}) \quad (10)$$

Eq. (10) can also be derived from Eq. (9) with $\bar{r}_p = 0$. A similar form to Eq. (10) has been obtained for a concentrated load acting at the center of a circular isotropic linear elastic plate [38,40].

In another limiting case of $\omega \to \infty$ (infinitely large membrane tension or negligible bending rigidity) which might not be physiologically relevant, Eqs. (6) and (7) reduce to

$$f = -\frac{2\pi\kappa_0\omega^2}{R^2\ln\bar{r}_p}L \quad \text{and} \quad z = \frac{\ln\bar{r}}{\ln\bar{r}_p}L$$

resulting in

$$z = -\frac{f R^2}{2\pi\kappa_0\omega^2}\ln\bar{r}$$

Our previous study [28] on the pulling of a homogeneous membrane indicates that increasing the pulling region size r_p leads to an increasing f_{max}, and moreover, as r_p increases, the *f*–*L* profile changes from a smooth and continuous curve to a discontinuous curve (Fig. 2(*a*)). Such features are also observed for the extraction of the multicomponent membrane considered here (Fig. 2(*a*)). As r_p increases, the energy profile exhibits a kink at a critical *L*/*R* (see Fig. S1 available in the Supplemental Materials on the ASME Digital Collection), corresponding to a discontinuous membrane shape transformation from the catenoid-like shape to the tubular structure. Additional calculations on the effects of r_p and α on the *f*–*L* curve and the order parameter profile can be found in Figs. S2 and S3, respectively. One more intriguing phenomenon is that the sudden drop in the force *f* could occur immediately following the force peak f_{max} at finite α as r_p increases (see the blue dotted line with rectanglar marker in Fig. 2(*a*) and a comparison between Figs. S2(*a*) and S2(*b*)). This indicates again that the composition coupling to the bending rigidity facilitates the membrane nanotube formation.

We next investigate the effects of the membrane tension on the membrane extraction. In our previous study on the pulling of a homogeneous membrane, we show that as the membrane tension increases, both the force peak and the plateau force increase, and the force drop occurs at smaller *L*/*R* [28]. A similar feature is offered during the pulling of multicomponent membranes (Fig. 4). Since the coupling parameter α is finite here, the force drop occurs immediately following the force peak at a finite r_p of $0.1R$ consistent with Figs. 2(*a*) and S2. In the case of $\alpha = 0.5$ and

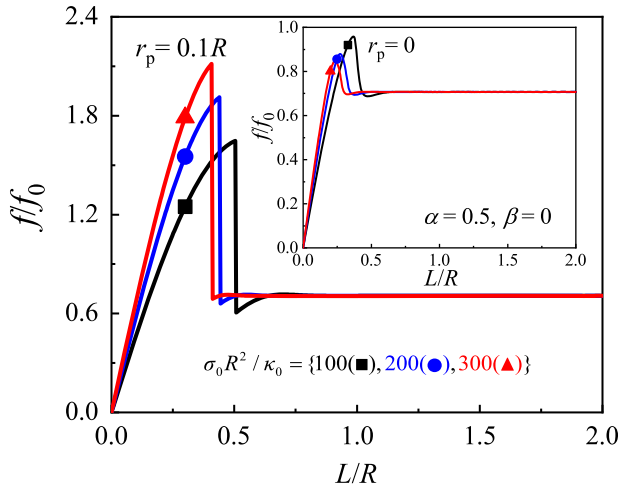

Fig. 4 The *f*–*L* curves for different membrane tension $\sigma_0 R^2/\kappa_0 = 100$, 200, and 300 at $\alpha = 0.5$ and $\beta = 0$ with $f_0 = 2\pi\sqrt{2\sigma_0\kappa_0}$ (Color version online.)

$\beta = 0$, the plateau force equals to $2\pi\sqrt{2\sigma_0\kappa_0}$ at small membrane tension $\sigma_0 = 25\kappa_0/R^2$ (Fig. S4); in other words, the membrane nanotube is in L_o phase with $\phi = 1$. This means that the phase separation never occurs if the membrane tension is small enough.

To demonstrate more clearly, the effects of the coupling between the membrane composition and mechanical properties, pulling region size, and membrane tension on the force barrier, we plot the normalized maximum pulling force differences $(f_{max}^{(\alpha=0)} - f_{max}^{(\alpha=0.5)})/f_0$ as functions of $\bar{r}_p$ at different σ_0 R^2/κ_0 and $\beta = 0$ with $f_0 = 2\pi\sqrt{2\sigma_0\kappa_0}$ in Fig. 5. It is shown that at small $\bar{r}_p$, the coupling of composition and flexibility plays an important role in regulating the membrane extraction, and such an effect due to the phase separation diminishes gradually as the pulling region enlarges and the force barrier becomes dominated by $\bar{r}_p$ of a relatively large value. Though in the numerical studies here, we consider a wide range of $\bar{r}_p \in [0, 0.2]$ for systematic analysis, $\bar{r}_p (\equiv r_p/R)$ in most biological circumstances is very small [15,17,20,27]. For example, it is reported that $\bar{r}_p \approx 0.018$ ($r_p = 100$ nm and $R \sim 5.6$ μm) in the pulling of a nanotube from lipid mixture vesicles [15]; $\bar{r}_p \to 0$ with a pulling region size around 55 nm for supported cells [27]. In these cases, the coupling effect cannot be simply ignored as indicated in Fig. 5.

To understand how the membrane patch size affects the membrane extraction, we perform case studies at different patch radii (R, $2R$, and $3R$) (see Fig. S5). In the case of point pulling force ($r_p = 0$), though the force peak f_{max} does not change, the extraction displacement L at which the force reaches a peak increases as the membrane size increases, namely, the formation of the membrane nanotube is delayed. At finite r_p, an increasing patch size induces a slightly decreasing f_{max}.

Having knowledge of the f–L curves at different membrane tensions and pulling region sizes (Figs. 2(*a*), 4, S2, S4, S5), we could determine the dependence of f_{max} on r_p at different σ. Two groups of the dependence have been found (Fig. 6). In the first group, the symbols refer to the cases of no coupling ($\alpha = 0$) with arbitrary r_p and the cases of $\alpha = 0.5$ with $r_p = 0$, and all these symbols collapse onto a single master curve (dotted line in Fig. 6), corresponding to the cases in which the force drop does not immediately follow the peak f_{max} such as the curves in Fig. 2(*a*) marked by the circles, triangles, and diamonds. The dotted line can be approximated by an empirical equation as [28]

$$\frac{r_p}{r_{\alpha\beta}} = B_1\left(\frac{f_{max}}{f_{\alpha\beta}} - \bar{f}\right) + \sqrt{\left(\frac{f_{max}}{f_{\alpha\beta}} - \bar{f} + B_2\right)^2 - B_2^2}$$

where $f_{\alpha\beta} = 2\pi\sqrt{2\sigma_0\kappa_0(1-\alpha)(1-\beta)}$, $r_{\alpha\beta} = \sqrt{\kappa_0(1-\alpha)/[\sigma_0(1-\beta)]}$, $B_1 = 28/29$, $B_2 = 7/17$, and $\bar{f} = 1.1267$. In the case of a point pulling force ($r_p = 0$), $f_{max}/f_0 = \bar{f}$. At large r_p, the above empirical equation can be estimated by a simple linear equation $f_{max}/f_0 = 1 + r_p/(2r_{\alpha\beta})$ which was first proposed by Koster et al. for the extraction of a homogeneous lipid membrane [20]. The second group refers to the cases of $\alpha = 0.5$ with finite r_p (the rest three colored solid lines in Fig. 6), and the symbols therein correspond to the cases in which the force drop immediately follows f_{max} such as the curves in Fig. 4 at $r_p = 0.1R$. Though the curves of $f_{max}/f_{\alpha\beta}$ as functions of $r_p/r_{\alpha\beta}$ at different σ_0 exhibit linear feature, their slopes are slightly different and they do not collapse together.

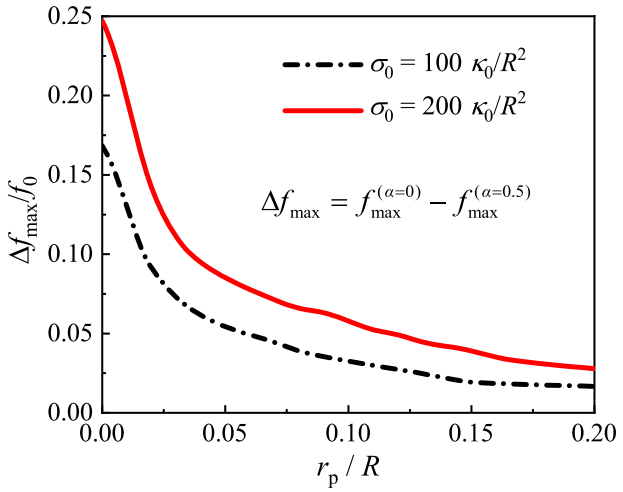

Fig. 5 Normalized maximum pulling force differences $(f_{max}^{(\alpha=0)} - f_{max}^{(\alpha=0.5)})/f_0$ as functions of $\bar{r}_p (\equiv r_p/R)$ at different σ_0 R^2/κ_0 and $\beta = 0$ with $f_0 = 2\pi\sqrt{2\sigma_0\kappa_0}$ (Color version online.)

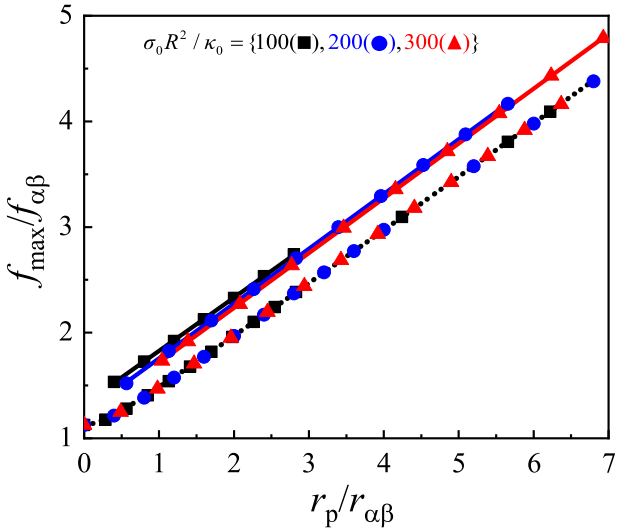

Fig. 6 Plots of the normalized maximum pulling force $f_{max}/f_{\alpha\beta}$ as a function of $r_p/r_{\alpha\beta}$ at different σ_0 R^2/κ_0 with $f_{\alpha\beta} = 2\pi\sqrt{2\sigma_0\kappa_0(1-\alpha)(1-\beta)}$ and $r_{\alpha\beta} = \sqrt{\kappa_0(1-\alpha)/[\sigma_0(1-\beta)]}$. Here, we take $\beta = 0$ in our case studies. The data collapsing onto the dotted curve correspond to the cases where the force drop does not immediately follow the peak f_{max} ($\alpha = 0$ with arbitrary r_p and $\alpha = 0.5$ with $r_p = 0$), while other symbols correspond to cases where the force drop immediately follows f_{max} ($\alpha = 0.5$ with finite r_p). (Color version online.)

To investigate the effect of coupling between the membrane composition and tension on the extraction, we now consider the f–L curves with finite β at $\sigma_0 = 200\kappa_0/R^2$ and $r_p = 0.2R$ and compare them with the cases of $\beta = 0$ at the same σ_0 and r_p in Fig. 2(*a*). The common feature shared by these four curves is that the force rises to a peak force which is followed by a drop to a plateau upon the formation of a membrane nanotube (Fig. 7). In the case of no coupling ($\alpha = \beta = 0$), the plateau force is $f_0 = 2\pi\sqrt{2\sigma_0\kappa_0}$; in the rest cases in Fig. 7, the plateau forces become lower and stay at $f_{\alpha\beta} = 2\pi\sqrt{2\sigma_0\kappa_0(1-\alpha)(1-\beta)}$. Difference in the plateau force from the no coupling case means that the membrane undergoes lipid phase separation during the extraction, which can be used as a criterion for the occurrence of lipid sorting complementary to the direct experimental observation. Moreover, the membrane tension is reduced by a factor $1-\beta$ as $\beta \in (0, 1)$ ($\beta = 0.5$ in our studies), leading to a lower slope in the early stage of the f–L curve and a lower force peak. The force curves at finite β in the case of the point pulling force is shown in Fig. S6 where no kink (or discontinuous shape transformation) is observed.

In this work, we focus on the extraction of a free membrane. For a supported membrane bonded to a substrate such as functionalized solid surface and underlying cytoskeleton, the membrane would undergo detachment from the substrate against the adhesive interaction. In the case of specific adhesion, the pulling force exhibiting a rate-dependent feature increases as the loading rate increases [41,42]. For an extremely soft substrate [43], the elastic deformation and mechanical instability of the substrate surface might play a significant role in manipulating the membrane nanotube formation.

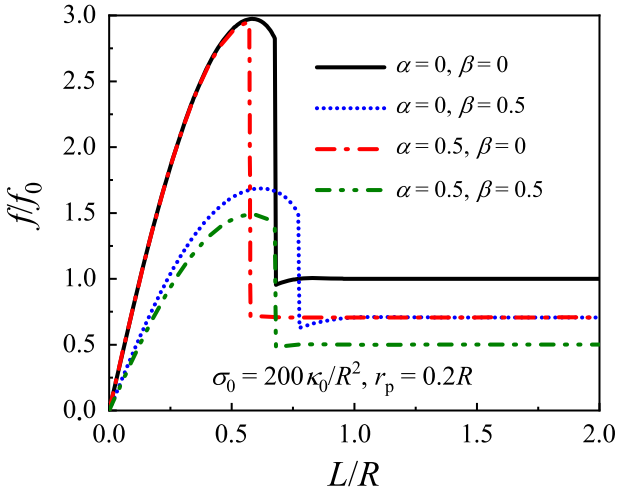

Fig. 7 The *f*–*L* curves of different coupling parameters at $\sigma_0 = 200\kappa_0/R^2$ and $r_p = 0.2R$ (Color version online.)

Membrane tension could vary in a wide range from 10^{-5} mN/m to 1 mN/m as reported [44]. Previous theoretical studies on the average force exerted by a thermally fluctuating membrane nanotube indicate that the thermal fluctuation of the membrane lowers the axial force $f_0 = 2\pi\sqrt{2\sigma\kappa}$ by an amount of Δf [45,46]. At high membrane tension (>0.01 mN/m), Δf is negligible; at low-to-moderate membrane tension (<10^{-4} mN/m), Δf is comparable with f_0 [45,46]. Therefore, strictly speaking, the thermal fluctuation would induce a lower plateau force and facilitate the membrane nanotube formation. A thorough theoretical analysis on the effect of thermal fluctuation to the pulling behavior of a homogeneous or multicomponent membrane is certainly deserved in the future study.

Our current studies are restricted to the quasi-static cases. At a finite pulling velocity, the membrane viscosity, inter-monolayer slip, and possible membrane slip over the cytoskeleton could together play significant roles in manipulating the membrane extraction [47–49]. Recent experiments have demonstrated that the phase separation during the membrane extraction also depends on the pulling velocity [17]. At a low pulling velocity, the lipid or protein flow is negligible in comparison with the lipid or protein diffusion [18]. Therefore, the phase separation is dominated by the elastic deformation energy of the system, and the L_d phase aggregates into the membrane tubule induced by the external extraction as our current quasi-static analysis indicates. At a high pulling velocity, the membrane is far from the equilibrium state and the extracted membrane stays in a L_o rather than L_d phase as a whole [17,18]. After the pulling stops, one L_d phase domain nucleates and expands around the neck of the membrane nanotube which connects the catenoid-like outer membrane region and exhibits a slight constriction. As the L_d phase domain expands, the pulling force decreases until the whole membrane nanotube is in the L_d phase [17,18]. Further investigation indicates that the L_o phase domain and L_d phase domain arrange in the membrane nanotube alternately at an intermediate speed [17], as a result of the competition between the curvature-modulated lipid diffusion and pulling-driven lipid flow. For a homogeneous membrane, experimental studies [47,48] and numerical calculations [49] indicate that the effective viscosity of the membrane nanotube and the pulling force follows a linear relationship in a physiological range of the pulling speed. Further studies are required to explore whether the linear relationship is valid for a multicomponent membrane.

Introducing an energy term associated with the difference of the principal membrane curvatures, our current model can be generalized to the cases with anisotropy of membrane components which could be membrane-attached proteins and macromolecules with anisotropic properties [50].

4 Conclusions

We have performed a theoretical study on the formation of the multicomponent membrane nanotube and the associated curvature-driven lipid sorting and explore the dependence on the size of the pulling region. The pulling force required for the membrane extraction increases first almost linearly with the pulling displacement and then drops and saturates at a value depending on the coupling between the membrane composition and the bending rigidity and tension of membrane upon the formation of a membrane nanotube. During the membrane extraction, the more flexible lipid-disordered phase aggregates into the tubular domain of a relatively large local curvature, and the outer membrane region stays in a lipid-ordered phase as long as the phase separation occurs. Moreover, the coupling between the membrane bending rigidity and membrane composition facilitates the formation of the membrane nanotube by reducing the force barrier. The maximum pulling force f_{max} is proportional to the size of the pulling region r_p. For a homogeneous membrane or at a point pulling force, f_{max} and r_p follow a nonlinear relationship independent of the membrane tension, while for a multicomponent membrane at a finite r_p, the f_{max}–r_p relationship depends on the membrane tension. These results indicate that the finite pulling region size cannot be ignored in approaching biophysical contexts such as the bundle of microtubules polymerizing underneath cell membranes and membrane extraction by clusters of motor proteins. Analytical solutions for the force-extraction relation and the membrane configuration in the early stage of the membrane extraction are obtained based on the nonlinear plate theory. Our results establish a correlation between the lipid sorting and membrane nanotube formation and shed light on the mechanical behaviors of multicomponent cell membranes associated with tubular deformation such as filopodial growth, cell uptake of one-dimensional nanomaterials such as gold nanowires and asbestos nanofibers, protein-mediated endocytosis, or vesiculation.

Funding Data

- National Natural Science Foundation of China (Grant Nos. 11872005 and 11521202; Funder ID: 10.13039/501100001809).

References

[1] Veatch, S. L., and Keller, S. L., 2003, "Separation of Liquid Phases in Giant Vesicles of Ternary Mixtures of Phospholipids and Cholesterol," Biophys. J., **85**(5), pp. 3074–3083.

[2] Baumgart, T., Hess, S. T., and Webb, W. W., 2003, "Imaging Coexisting Fluid Domains in Biomembrane Models Coupling Curvature and Line Tension," Nature, **425**(6960), pp. 821–824.

[3] Jensen, U. B., Ferapontova, E. E., and Sutherland, D. S., 2012, "Quantifying Protein Adsorption and Function At Nanostructured Materials: Enzymatic Activity of Glucose Oxidase At GLAD Structured Electrodes," Langmuir, **28**(30), pp. 11106–11114.

[4] Hu, J., Weikl, T., and Lipowsky, R., 2011, "Vesicles With Multiple Membrane Domains," Soft. Matter, **7**(13), pp. 6092–6102.

[5] Simons, K., and Vaz, W. L., 2004, "Model Systems, Lipid Rafts, and Cell Membranes," Annu. Rev. Biophys. Biomol. Struct., **33**(1), pp. 269–295.

[6] Howell, A. S., and Lew, D. J., 2012, "Morphogenesis and the Cell Cycle," Genetics, **190**(1), pp. 51–77.

[7] Kukulski, W., Schorb, M., Kaksonen, M., and Briggs, J., 2012, "Plasma Membrane Reshaping During Endocytosis is Revealed by Time-Resolved Electron Tomography," Cell, **150**(3), pp. 508–520.

[8] Różycki, B., Weikl, T. R., and Lipowsky, R., 2008, "Stable Patterns of Membrane Domains At Corrugated Substrates," Phys. Rev. Lett., **100**(9), p. 098103.

[9] Parthasarathy, R., Yu, C., and Groves, J. T., 2006, "Curvature-Modulated Phase Separation in Lipid Bilayer Membranes," Langmuir, **22**(11), pp. 5095–5099.

[10] Subramaniam, A. B., Lecuyer, S., Ramamurthi, K. S., Losick, R., and Stone, H. A., 2010, "Particle/fluid Interface Replication As a Means of Producing Topographically Patterned Polydimethylsiloxane Surfaces for Deposition of Lipid Bilayers," Adv. Mater., **22**(19), pp. 2142–2147.

[11] Hsieh, W.-T., Hsu, C.-J., Capraro, B. R., Wu, T., Chen, C.-M., Yang, S., and Baumgart, T., 2012, "Curvature Sorting of Peripheral Proteins on Solid-Supported Wavy Membranes," Langmuir, **28**(35), pp. 12838–12843.

[12] Rustom, A., Saffrich, R., Markovic, I., Walther, P., and Gerdes, H.-H., 2004, "Nanotubular Highways for Intercellular Organelle Transport," Science, **303**(5660), pp. 1007–1010.

[13] Arjonen, A., Kaukonen, R., and Ivaska, J., 2011, "Filopodia and Adhesion in Cancer Cell Motility," Cell Adh. Migr., **5**(5), pp. 421–430.
[14] Roux, A., Cuvelier, D., Nassoy, P., Prost, J., Bassereau, P., and Goud, B., 2005, "Role of Curvature and Phase Transition in Lipid Sorting and Fission of Membrane Tubules," EMBO J., **24**(8), pp. 1537–1545.
[15] Tian, A., and Baumgart, T., 2009, "Sorting of Lipids and Proteins in Membrane Curvature Gradients," Biophys. J., **96**(7), pp. 2676–2688.
[16] Jiang, H., and Powers, T. R., 2008, "Curvature-Driven Lipid Sorting in a Membrane Tubule," Phys. Rev. Lett., **101**(1), p. 018103.
[17] Heinrich, M., Tian, A., Esposito, C., and Baumgart, T., 2010, "Dynamic Sorting of Lipids and Proteins in Membrane Tubes With a Moving Phase Boundary," Proc. Natl. Acad. Sci. U.S.A., **107**(16), pp. 7208–7213.
[18] Jiang, H., 2012, "Dynamic Sorting of Lipids and Proteins in Multicomponent Membranes," Phys. Rev. Lett., **109**(19), p. 198101.
[19] Simunovic, M., Manneville, J.-B., Renard, H.-F., Evergren, E., Raghunathan, K., Bhatia, D., Kenworthy, A. K., Voth, G. A., Prost, J., McMahon, H. T., Johannes, L., Bassereau, P., and Callan-Jones, A., 2017, "Friction Mediates Scission of Tubular Membranes Scaffolded by Bar Proteins," Cell, **170**(1), pp. 172–184.
[20] Koster, G., Cacciuto, A., Derényi, I., Frenkel, D., and Dogterom, M., 2005, "Force Barriers for Membrane Tube Formation," Phys. Rev. Lett., **94**(6), p. 068101.
[21] Koster, G., VanDuijn, M., Hofs, B., and Dogterom, M., 2003, "Membrane Tube Formation From Giant Vesicles by Dynamic Association of Motor Proteins," Proc. Natl. Acad. Sci. U.S.A., **100**(26), pp. 15583–15588.
[22] Johannes, L., and Mayor, S., 2010, "Induced Domain Formation in Endocytic Invagination, Lipid Sorting, and Scission," Cell, **142**(4), pp. 507–510.
[23] Farsad, K., and Camilli, P. D., 2003, "Mechanisms of Membrane Deformation," Curr. Opin. Cell Biol., **15**(4), pp. 372–381.
[24] Zhu, Q., Zheng, F., Liu, A. P., Qian, J., Fu, C., and Lin, Y., 2016, "Shape Transformation of the Nuclear Envelope During Closed Mitosis," Biophys. J., **111**(10), pp. 2309–2316.
[25] Powers, T. R., Huber, G., and Goldstein, R. E., 2002, "Fluid-Membrane Tethers: Minimal Surfaces and Elastic Boundary Layers," Phys. Rev. E, **65**(4), p. 041901.
[26] Derényi, I., Jülicher, F., and Prost, J., 2002, "Formation and Interaction of Membrane Tubes," Phys. Rev. Lett., **88**(23), p. 238101.
[27] Pontes, B., Viana, N., Salgado, L., Farina, M., Neto, V. M., and Nussenzveig, H., 2011, "Cell Cytoskeleton and Tether Extraction," Biophys. J., **101**(1), pp. 43–52.
[28] Tian, F., Yue, T., Dong, W., Yi, X., and Zhang, X., 2018, "Size-Dependent Formation of Membrane Nanotubes: Continuum Modeling and Molecular Dynamics Simulations," Phys. Chem. Chem. Phys., **20**(5), pp. 3474–3483.
[29] Yi, X., Zou, G., and Gao, H., 2018, "Mechanics of Cellular Packing of Nanorods With Finite and Non-Uniform Diameters," Nanoscale, **10**(29), pp. 14090–14099.
[30] Li, S., Yan, Z., Luo, Z., Xu, Y., Huang, F., Zhang, X., Yi, X., and Yue, T., 2019, "Mechanics of the Formation, Interaction, and Evolution of Membrane Tubular Structures," Biophys. J., **116**(5), pp. 884–892.
[31] Helfrich, W., 1973, "Elastic Properties of Lipid Bilayers: Theory and Possible Experiments," Z. Naturforsch. C, **28**(11–12), pp. 693–703.
[32] Tsafrir, I., Sagi, D., Arzi, T., Guedeau-Boudeville, M.-A., Frette, V., Kandel, D., and Stavans, J., 2001, "Pearling Instabilities of Membrane Tubes With Anchored Polymers," Phys. Rev. Lett., **86**(6), pp. 1138–1141.
[33] Allain, J.-M., Storm, C., Roux, A., Amar, M. B., and Joanny, J.-F., 2004, "Fission of a Multiphase Membrane Tube," Phys. Rev. Lett., **93**(15), p. 158104.
[34] Leibler, S., and Andelman, D., 1987, "Ordered and Curved Meso-Structures in Membranes and Amphiphilic Films," J. Phys., **48**(11), pp. 2013–2018.
[35] Zou, G., Yi, X., Zhu, W., and Gao, H., 2018, "Packing of Flexible Nanofibers in Vesicles," Extreme Mech. Lett., **19**(Mar.), pp. 20–26.
[36] Fournier, J.-B., 2007, "On the Stress and Torque Tensors in Fluid Membranes," Soft Matter, **3**(7), pp. 883–888.
[37] Deserno, M., Müller, M. M., and Guven, J., 2007, "Contact Lines for Fluid Surface Adhesion," Phys. Rev. E, **76**(1), p. 011605.
[38] Timoshenko, S., and Woinowsky-Krieger, S., 1959, *Theory of Plates and Shells*, McGraw-Hill, New York.
[39] Wan, K.-T., 1999, "Fracture Mechanics of a Shaft-Loaded Blister Test Transition From a Bending Plate to a Stretching Membrane," J. Adhes., **70**(3–4), pp. 209–219.
[40] Wan, K.-T., 2002, "Adherence of An Axisymmetric Flat Punch Onto a Clamped Circular Plate: Transition From a Rigid Plate to a Flexible Membrane," ASME J. Appl. Mech., **69**(2), pp. 110–116.
[41] Lin, Y., and Freund, L., 2007, "Forced Detachment of a Vesicle in Adhesive Contact With a Substrate," Int. J. Solids Struct., **44**(6), pp. 1927–1938.
[42] Lin, J., Lin, Y., and Qian, J., 2014, "Statistical Pull Off of Nanoparticles Adhering to Compliant Substrates," Langmuir, **30**(21), pp. 6089–6094.
[43] Li, B., Cao, Y.-P., Feng, X.-Q., and Gao, H., 2012, "Mechanics of Morphological Instabilities and Surface Wrinkling in Soft Materials: A Review," Soft Matter, **8**(21), pp. 5728–5745.
[44] Morris, C., and Homann, U., 2001, "Cell Surface Area Regulation and Membrane Tension," J. Membr. Biol., **179**(2), pp. 79–102.
[45] Fournier, J.-B., and Galatola, P., 2007, "Critical Fluctuations of Tense Fluid Membrane Tubules," Phys. Rev. Lett., **98**(1), p. 018103.
[46] Barbetta, C., and Fournier, J.-B., 2009, "On the Fluctuations of the Force Exerted by a Lipid Nanotubule," Eur. Phys. J. E, **29**(2), pp. 183–189.
[47] Evans, E., and Yeung, A., 1994, "Hidden Dynamics in Rapid Changes of Bilayer Shape," Chem. Phys. Lipids, **73**(1), pp. 39–56.
[48] Hochmuth, F., Shao, J., Dai, J., and Sheetz, M., 1996, "Deformation and Flow of Membrane Into Tethers Extracted From Neuronal Growth Cones," Biophys. J., **70**(1), pp. 358–369.
[49] Rahimi, M., and Arroyo, M., 2012, "Shape Dynamics, Lipid Hydrodynamics, and the Complex Viscoelasticity of Bilayer Membranes," Phys. Rev. E, **86**(1), p. 011932.
[50] Bobrovska, N., Góźdź, W., Kralj-Iglič, V., and Iglič, A., 2013, "On the Role of Anisotropy of Membrane Components in Formation and Stabilization of Tubular Structures in Multicomponent Membranes," PLoS One, **8**(9), p. e73941.

Supplemental Materials for "Force Barrier for Lipid Sorting in the Formation of Membrane Nanotubes"

Xingyi Tang[a], Jianxiang Wang[a,b,1], Xin Yi[a,c,1]
[a]Department of Mechanics and Engineering Science, College of Engineering,
Peking University, Beijing 100871, China
[b]CAPT-HEDPS and IFSA Collaborative Innovation Center of MoE, College of Engineering,
Peking University, Beijing 100871, China
[c]Beijing Innovation Center for Engineering Science and Advanced Technology,
Peking University, Beijing 100871, China
[1]E-mails: jxwang@pku.edu.cn; xyi@pku.edu.cn

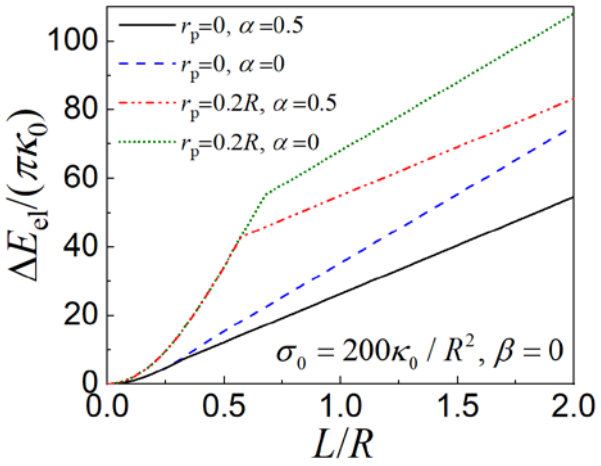

Fig. S1. Variation of the elastic deformation energy $\Delta E_{el} = E_{tot}(L) - E_{tot}(0)$ as a function of L/R at different r_p and α.

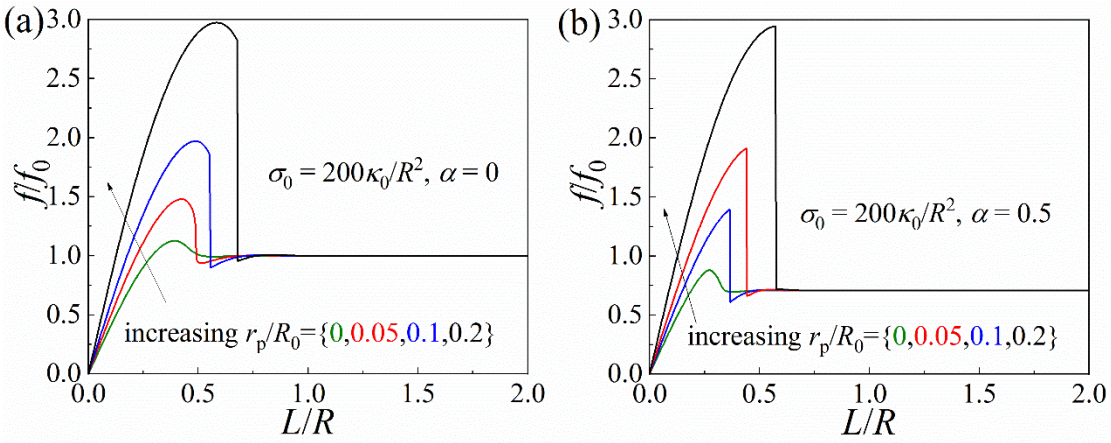

Fig. S2. Effects of the pulling region size r_p on the f-L curves at α=0 (a) and 0.5 (b). Here $f_0 = 2\pi\sqrt{2\sigma_0\kappa_0}$, σ_0=200κ_0/R^2, and β=0.

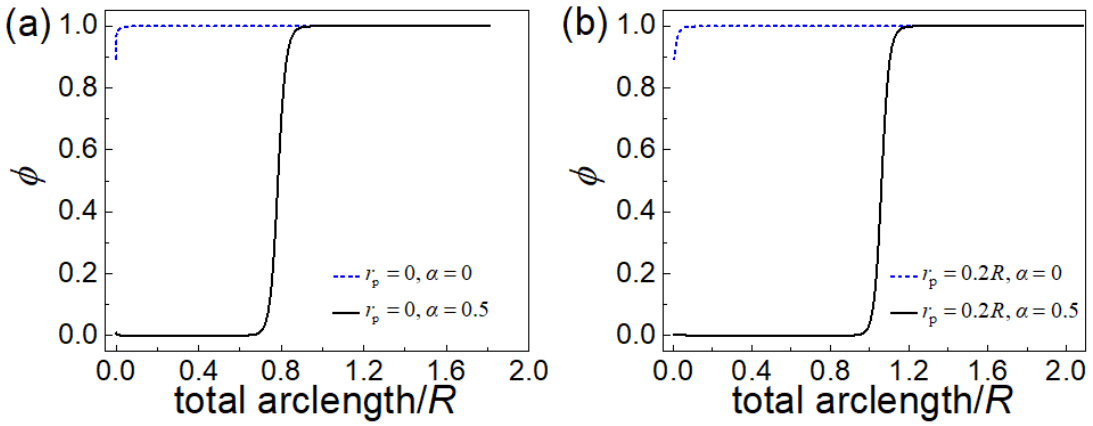

Fig. S3. The evolution of the order parameter ϕ as a function of the normalized total arclength including the membrane on the pulling region at r_p=0 (a) and 0.2R (b). Here we take σ_0=200κ_0/R^2, β=0, and L/R=1.

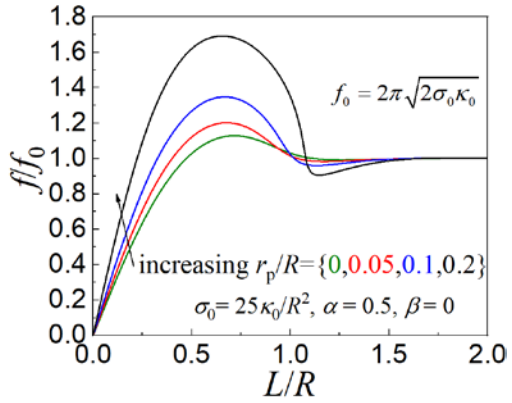

Fig. S4. Effects of the pulling region size r_p on the f-L curves at relatively small membrane tension σ_0=25κ_0/R^2. Here we take α=0.5 and β=0. For α smaller than 0.5, no distinguishable differences are found from the f-L curves in this figure.

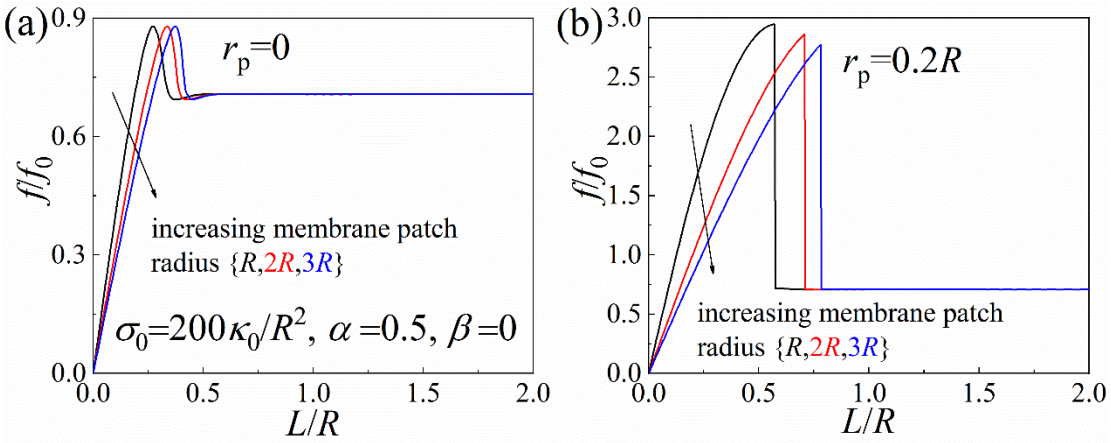

Fig. S5. Effects of the membrane patch size on the f-L curves at r_p=0 and 0.2R with $f_0 = 2\pi\sqrt{2\sigma_0\kappa_0}$. Here we take σ_0=200κ_0/R^2, α=0.5, and β=0.

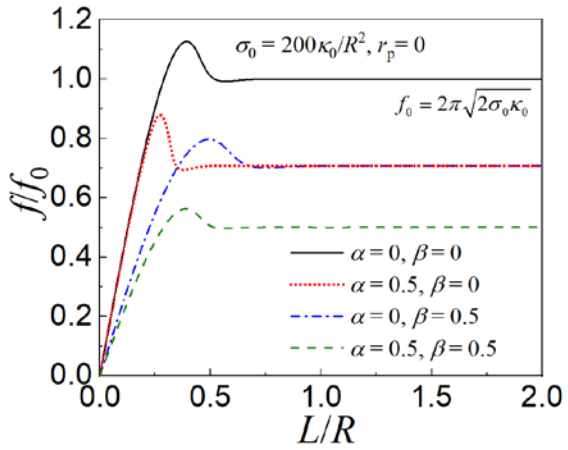

Fig. S6. The *f*-*L* curves for the point pulling force (r_p=0) at different sets of the coupling parameters (α,β).